10

Near-infrared emitting $NaLuF_4$: Yb^{3+}, Er^{3+}, Ce^{3+} nanoparticles for compact waveguide amplifiers and bioimaging

© K.V. Khaydukov[1,3], I.V. Krylov[1], M.E. Nikolaeva[2,3], V.V. Rocheva[1], E.V. Khaydukov[1,3,¶]

[1] Federal Research Center „Crystallography and Photonics", Russian Academy of Sciences, Moscow, Russia
[2] Research and Production Company „NPF LLC Sintol",
127434 Moscow, Russia
[3] Moscow Pedagogical State University, Moscow, Russia

¶ E-mail: khaydukov@mail.ru

Received November 23, 2022
Revised February 20, 2023
Accepted February 22, 2023

Fluoride nanocrystals co-doped with lanthanide ions are well known due to the possibility of conversion near-infrared (NIR) radiation into photoluminescence with large anti-Stokes shift. Owing to upconversion effect, such nanomaterials have shown great potential in photonics and biomedicine. However, fluoride nanoparticles can be reconfigured to photoluminescence with a Stokes shift into the near-infrared region of the spectrum. In this work, we focused on the properties of $NaRF_4:Yb^{3+}$, Er^{3+}, Ce^{3+} (R = Y, Lu) nanoparticles exhibiting intense stokes luminescence in the vicinity of 1530 nm at 975 nm excitation. Photoluminescence quantum efficiency of synthesized nanoparticles was evaluated as 28% at 0.6 W/cm^2 excitation intensity. Based on the photoluminescent properties of nanoparticles we designed compact waveguide amplifier for C-band telecommunication and developed time gated imaging system for NIR-to-NIR biovisualization.

Keywords: waveguide amplifier, fluoride nanocrystals, bioimaging, polymer waveguides, $NaLuF_4:Yb^{3+}$, Er^{3+}, Ce^{3+}.

DOI: 10.61011/EOS.2023.05.56514.75-22

1. Introduction

Photoluminescent materials doped with trivalent lanthanide ions, which have the electronic configuration $4f^n5s^25p^6$ with $n = 0.14$ for $R^{3+} = La-Lu$, are attracting considerable attention due to their unique physical properties [1–4]. The partially filled $4f$ shell causes the presence of a large number of metastable energy levels in the IR, visible, and UV areas of the spectrum. Due to the shielding of internal $4f$ electrons by outer filled $5s$- and $5p$ shells, the position of the energy levels of lanthanide ions is weakly affected by the crystal field of the matrix and external conditions [2,5,6]. An important role in the efficiency of the process of photoluminescence of lanthanide ions is played by the choice of the crystal matrix material, which should have a high transmittance, high isomorphic capacity of the crystal matrix with respect to activator ions, and high chemical and thermal stability [2,6.8]. Comparison of the known classes of wide-band oxygen-containing and halide crystalline compounds shows that only materials based on inorganic fluorides most fully satisfy the above requirements [2,6].

The significance of the class of fluoride nanomaterials is well shown for the implementation of the up-conversion process [2,6,9]. The best up-conversion efficiency $\sim 1-10\%$ was achieved in fluoride crystalline matrices, for example, $NaYF_4$, SrF_2, BaF_2, co-doped with a pair of trivalent lanthanide ions $Yb^{3+}Er^{3+}$ and $Yb^{3+}Tm^{3+}$ [10–13]. Due to the relatively high efficiency of converting near-IR light into higher-energy photons, this class of nanomaterials has found wide application in photonics and biomedicine. For example, 3D displays [14,15], nanosensors [16,17], anti-counterfeit tags [18,19], solar cells [20], 3D printing [21], ultra-high resolution optical microscopy [22], retroemission devices [23], fingerprinting [24], diagnostic and therapeutic nanostructures [25].

On the other hand, this class of nanoparticles can be used to obtain stokes-shifted photoluminescence, the so-called down conversion process [26]. The down-conversion process consists of the same processes as up-conversion. The difference is that the sensitizer transfers the absorbed energy to the activator, the activator nonradiatively passes to a metastable energy level with subsequent radiative relaxation to the ground state. Meanwhile, the successive population of high-lying energy states of the activator ion is limited. In nanoparticles co-doped with a pair of trivalent lanthanide ions, a wavelength difference between the absorbed and emitted photons of more than 500 nm can be achieved. To implement the down-conversion, as in the up-conversion, it is preferable to use the Yb^{3+} ion as a sensitizer ion, since the absorption cross section of the $^2F_{5/2} \rightarrow {}^2F_{7/2}$ transition in nanoparticles at a wavelength of 975 nm can reach the value $2 \cdot 10^{-19}$ cm^2 [27]. Er^{3+} ion as an activator ion, which, due to the unique structure of energy levels, allows to obtain both stokes and anti-stokes photoluminescence [28]. Additionally, $^{3+}$ ions can be introduced into the system, which are capable of accelerating the process of populating the lower-lying energy state of the activator ion, hindering

the excitation energy drain through the up-conversion channel [29]. In general, the down conversion process has a higher quantum efficiency [3] than up-conversion and, more importantly, a linear dependence of the photoluminescence intensity on the excitation intensity [26]. One of the brightest applications where nanoparticles co-doped with Yb^{3+}, Er^{3+}, Ce^{3+} ions, due to intense photoluminescence in the vicinity of 1530 nm upon excitation at 975 nm, can find application is bioimaging in the near-IR spectral region (1000−1700 nm) and the creation of compact waveguide amplifiers for the C-telecommunication band.

In this paper, the nanoparticles β-$NaLuF_4:Yb^{3+}$, Er^{3+}, β-$NaYF_4:Yb^{3+}$, Er^{3+}, Ce^{3+} and β-$NaLuF_4:Yb^{3+}$, Er^{3+}, Ce^{3+} were synthesized and investigated their photoluminescent properties in the near IR area of the spectrum. The opportunity of their application for optical imaging with delayed registration of the photoluminescence signal is shown, which seems promising for the tasks of marking biological objects due to its simplicity and low cost. Based on the SU-8 photoresist, a composite material containing $NaLuF_4:Yb^{3+}$, Er^{3+}, Ce^{3+}/$NaLuF_4$ nanoparticles was created, from which compact polymeric waveguides were fabricated by contact UV photolithography to amplify the optical signal in the vicinity of 1530 nm.

2. Methods

2.1. Synthesis of nanoparticles

Thermal decomposition of precursors, as one of the most efficient methods for synthesizing nanoparticles with high quantum efficiency, refers to a synthetic process in which organometallic precursors are dissolved in high-boiling organic solvents and then decomposed at elevated temperatures [2]. In this paper, we used the method of high-temperature decomposition of trifluoroacetates in an oxygen-free environment. The technique for synthesizing nanoparticles is based on the coordinate stabilization of metal precursor salts (sodium, yttrium, lutetium, ytterbium, erbium, and cerium) in an oleic acid solution, which takes place with heating in an oxygen-free medium. This approach was applied to the synthesis of nanoparticles with various fluoride crystal matrices β-$NaLuF_4$ and β-$NaYF_4$ co-doped with Yb^{3+}, Er^{3+}, Ce^{3+} ions. Reagents for the synthesis of nanoparticles were purchased from Merck: yttrium, lutetium, ytterbium and cerium oxides — ultrapure 99.99%, sodium trifluoroacetate — purity 97%, trifluoroacetic acid — purity 99%, octadecene — purity $\geq$ 90%, oleic acid — extra pure. For the synthesis of $NaYF_4$ nanoparticles: 18%Yb^{3+}, 2%Er^{3+}, 2%Ce^{3+} mixture was placed in a three-necked flask 286 mg Y_2O_3, 134 mg Yb_2O_3, 12.8 mg Er_2O_3, 71 mg $(CH_3COO)_3Ce$. 5 mL of trifluoroacetic acid and 1 mL of distilled water were added. The resulting mixture was boiled for 2 h until the precipitate was completely dissolved. Then the mixture was evaporated. The reaction for obtaining trifluoroacetates is written as

$$Y_2O_3 + Yb_2O_3 + Er_2O_3 + \\ + (CH_3COO)_3Ce \xrightarrow{CF_3COOH,H_2O)} (CH_3COO)_3Y + \\ + (CH_3COO)_3Yb + (CH_3COO)_3Er + (CH_3COO)_3Ce.$$

To a mixture of obtained trifluoroacetates $(CF_3COO)_3Y$, $(CF_3COO)_3Yb$, $(CF_3COO)_3Er$, $(CF_3COO)_3Ce$ 764 mL CF_3COONa were added. The solvents were evaporated, and the resulting mixture was dissolved in a minimum amount of methanol. Next, high-boiling solvents were poured into the flask: 15 mL 90% 1-octadecene and 15 mL 90% oleic acid. The resulting solution was heated to 100°C for 30 min under reduced pressure, which allowed to get rid of residual low-boiling solvents (water and methanol). There was dissolution of the precipitate. After 30 min, the solution was heated to 160°C at atmospheric pressure in an argon atmosphere. Next, the flask was heated to 340°C in Rose alloy. As a result of heating the mixture, the decomposition of the trifluoroacetates of the corresponding metals occurred with the release of freons:

$$(CF_3COO)_3Y + (CF_3COO)_3Yb + (CF_3COO)_3Er \\ + (CF_3COO)_3Ce + (CF_3COO)_3Na \\ \xrightarrow{T>340^\circ C} NaYF_4 : Yb^{3+}, Er^{3+}, Ce^{3+}.$$

After 30 min, the reaction was stopped by cooling the three-necked flask to room temperature. The resulting nanoparticles were centrifuged at 6000 rpm/s for 15 min and washed twice with isopropanol.

To improve the photoluminescent properties of the final synthesis product, the nanoparticles were coated with an inert $NaYF_4$ crystalline shell. For this, $NaYF_4:Yb^{3+}$, Er^{3+}, Ce^{3+} nanoparticles were dispersed in a mixture of octadecene/oleic acid 1 : 1 and 295 mg of sodium trifluoroacetate was added. The mixture was stirred under vacuum at 100° for 30 min. Then the mixture was heated in a three-necked flask to 290° at atmospheric pressure and left at this temperature for 40 min. Next, the solution was cooled to room temperature, the mixture was centrifuged at 6,000 rpm/s for 15 min. The precipitate was washed twice with isopropanol. As a result, nanoparticles with an active core/inert shell structure were obtained. The shell thickness was 5−7 nm. The shell coating procedure minimizes the influence of surface defects of nanocrystals, which leads to an increase in the quantum efficiency of photoluminescence in comparison with nanoparticles without an inert crystalline shell. Additionally, the inert shell hinders the nonradiative transfer of the excitation energy of nanocrystals to molecules that are part of the photocomposite and are capable of quenching the luminescence of nanocrystals. Nanoparticles of the composition β-$NaLuF_4:Yb^{3+}$, Er^{3+}, Ce^{3+} were synthesized in a similar way, replacing yttrium oxide with lutetium oxide.

2.2. Study of spectra and kinetics of photoluminescence of nanoparticles

The spectra and kinetics of photoluminescence of nanoparticles were studied using a Fluorolog-3 fluorimeter (HJY, France) equipped with an H10330-75 photomultiplier (Hamamatsu Photonics, Japan) with a spectral sensitivity in the range from 950 to 1750 nm. For excitation, an external source was used — ATC semiconductor laser with a wavelength of 975 nm (Semiconductor Devices, Russia). To analyze the photoluminescence kinetics of the synthesized nanoparticles, a WaveRunner 9104R digital storage oscilloscope (Teledyne LeCroy, USA) was additionally connected to the photomultiplier. To measure the spectra and kinetics of photoluminescence, the synthesized nanocrystals were dispersed in methylene chloride CH2Cl2 and placed in the cuvette section of the fluorimeter.

2.3. TEM, SEM and XRD characterization

The phase composition of nanoparticles was studied by X-ray powder diffraction (XRD) (Rigaku Miniflex 600, Japan) in the range of angles $10^\circ \leq 2\theta \leq 100^\circ$ with a scanning step of 1°. The resulting diffraction patterns were compared with the ICDD (International Center for Diffraction Data) database. The sizes and morphology of the synthesized nanocrystals were examined using a Tecnai Osiris transmission electron microscope (TEM). The photographs of a single-mode polymer waveguide with nanocrystals were obtained using a scanning electron microscope (SEM) LEO 1450 (Carl Zeiss, Germany).

2.4. Measurements of the quantum efficiency of nanoparticles

To measure the quantum efficiency of nanoparticles photoluminescence, an experimental setup based on an integrating sphere (Labsphere, USA) was used, the walls of which are coated with a Spectraflect scattering material with a low absorption coefficient in the range from 300 to 2000 nm. For excitation of the nanoparticles photoluminescence, an ATC semiconductor laser with a wavelength of 975nm (Semiconductor Devices, Russia) was used. Collimated radiation from a semiconductor laser was directed to a quartz cell filled with a colloidal solution of nanoparticles in decalin and located at the center of an integrating sphere. Neutral light filters were installed between the laser radiation collimator and the sphere, which allowed to change the excitation intensity of the sample.

An InGaAs camera (Hamamatsu C10633-23, Japan) was used as a photodetector for detecting the photoluminescence of nanoparticles and scattered laser radiation. Spectral sensitivity range of the camera is 900−1700 nm. The camera was mounted on the output flange of the integrating sphere with the possibility of installing bandpass interference filters (Semrock, USA) in front of the chamber, which suppress the excitation wavelength of nanoparticles.

The screen inside the integrating sphere ensured that only the photoluminescent signal scattered from the walls of the sphere hit the camera matrix, excluding direct reflections and glare of the laser beam at a wavelength of 975 nm. The laser radiation that passed through the sample was extracted from the sphere through a flange coaxial with the input flange. A PM10 photodetector (Coherent, USA) was installed behind the output flange to estimate the laser radiation power absorbed by the sample. After calibration, the quantum efficiency of the stokes photoluminescence of the synthesized nanoparticles was measured, which was determined in the spectral range 1400−1700 nm as

$$\eta = P_{\text{em}}/P_{\text{abs}}\,[\text{W}\cdot\text{W}^{-1}]\cdot 100\%,$$

where P_{em} — emitted power in the range from 1400 to 1700 nm, P_{abs} — absorbed power at a wavelength of 975 nm.

2.5. Manufacture of waveguides

A waveguide with inclusions of nanoparticles was manufactured using SU-8 2005 photoresist (Microresist, Germany) and polystyrene thermoplastic polymer (Polineftekhim, Russia).

The SU-8 photoresist was used to make light-guiding strands of the waveguide, and the top layer was made of polystyrene. The refraction index of a light-guiding core made of SU-8 at a wavelength of 1530 nm is $n_1 = 1.5705$, the refraction index of a sheath made of polystyrene is $n_2 = 1.5646$. A silicon wafer („VEI“ LLC) with an oxide layer with a thickness of $\sim 3.7\,\mu$m and a refraction index of $n_{SiO_2} = 1.444$ (1530 nm) was used as a substrate. The oxide layer acted as a sublayer with a lower refraction index than that of the light guide wire.

To create a nanocomposite material for the light-guiding strands of the waveguide, nanoparticles $NaLuF_4$, Yb^{3+}, Er^{3+}, $Ce^{3+}/NaLuF_4$ with a mass of 0.005 g were dispersed in 2 g of toluene. The resulting solution was subjected to ultrasonic dispersion for 3 h and then mixed with 5 mL of SU-8 2005 monomer. During the manufacture of the waveguides, the solvent was evaporated. The final concentration of nanoparticles in the SU-8 2005 photoresist was ~ 0.12 wt.%.

A four-stage process was used to form polymeric waveguides from liquid photocomposites by contact UV lithography. The first stage included the preparation of an adhesive layer on a silicon wafer in low pressure plasma (Deiner electronic, Germany). A buffer layer of polystyrene dissolved in chlorobenzene was deposited on the adhesive layer by spin-coating. The thickness of a buffer layer was $40\,\mu$m. Next, the photoresist Su-8 2005 with introduced nanoparticles was deposited on a polystyrene buffer layer. By adjusting the substrate rotation speed on the spin-coating unit, the thickness of the photoresist deposition was $5\,\mu$m. Then the sample was kept for 20 min at a temperature of 85°C to remove the solvent from the resulting film. The

second stage is required for the formation of light-guiding channels by contact photolithography. A photomask was superimposed on the surface of a silicon wafer coated with polymer and photoresist layers. Through the photomask, the photoresist was illuminated with UV radiation, which triggers the SU-8 crosslinking process. After exposure, the third step — solvent washing procedure was carried out. As a result, the uncrosslinked photoresist was removed from the substrate surface. At the last stage, the resulting waveguides were covered with a layer of polystyrene. By cleaving a silicon wafer with waveguides, the required sample length was reached. Before laser radiation was introduced into the waveguides, the end face was chipped off.

2.6. Imaging system with delayed registration of photoluminescence

To obtain images from nanocrystals in the range 1000−1700 nm, an experimental setup operating in the transluminescent mode was used. A sample containing nanoparticles $NaLuF_4$, Yb^{3+}, Er^{3+}, $Ce^{3+}/NaLuF_4$, was irradiated with a divergent beam at a wavelength of 975 nm from an ATC Laser semiconductor laser (Semiconductor devices, Russia). The image was recorded using an InGaAs camera (Hamamatsu C10633-23, Japan). The implementation of the delayed registration mode was carried out by synchronizing the signal from a mechanical chopper MC2000B (Thorlabs, USA) located between the camera lens and the CCD matrix of the camera with pulsed laser radiation exciting photoluminescence. At the moment when the camera matrix is covered by a rotating chopper disk, the sample containing nanoparticles is illuminated by laser radiation. Then, when the open segment of the rotating disk passes in front of the camera matrix, the semiconductor laser is switched off for background-free registration of the photoluminescent signal from the nanoparticles. That is, the excitation of nanoparticles and the registration of the photoluminescence signal occur in antiphase. By adjusting the phase and speed of rotation of the chopper disk, performed using a G5-54 pulse generator (USSR), it was possible to achieve suppression of parasitic laser illumination of the sample for observing only long-term photoluminescence from nanoparticles with a maximum at a wavelength of 1530 nm.

3. Results

3.1. Characterization of nanoparticles

The nanoparticle consists of a crystalline matrix and three types of lanthanide ions. An ion of the first type is a sensitizer capable of effectively absorbing a photon with a wavelength of 970−980 nm and passing from the ground state to an excited metastable state. In a nanoparticle, nonradiative resonant energy transfer is possible between an excited sensitizer ion and an ion of the second type, an activator. Radiative energy transfer from the excited sensitizer to the activator leads to the excitation of activator ions into a metastable state. In order to exclude sequential population of the higher energy states of the activator ion, it is required to add to the system an ion of the third type — a limiter, which can accelerate the process of populating the lower-lying energy state of the activator ion. Radiative relaxation of the activator state leads to stokes photoluminescence. This multistep process in nanoparticles is required to suppress the up-conversion process in order to increase the quantum efficiency in the stokes channel of photoluminescence. The efficiency of this process is determined by the inorganic crystalline matrix, the concentration of lanthanides in the matrix, and the overlap of the emission and absorption spectra of ions [2]. The Yb^{3+} ion is one of the most effective sensitizers with absorption in the vicinity of the wavelength 975 nm. Er^{3+} ions are used as activator ions, which provide photoluminescence in the vicinity of the wavelength 1530 nm, and Ce^{3+} ions [29] are used for resonant settling of their excited states. Fig. 1 shows a schematic representation of an individual nanoparticle and an energy diagram for trivalent ytterbium, erbium, and cerium ions in a crystalline matrix.

A photon at a wavelength of 975 nm is absorbed by the Yb^{3+} ion, transferring it to the excited state $^2F_{5/2}$. As a result of nonradiative resonant energy transfer, the Er^{3+} $^4I_{13/2}$ level is populated inside an individual crystalline nanoparticle with the opportunity of subsequent excitation of the overlying energy states. The Ce^{3+} ions are capable of resonantly settling the energy states of Er^{3+} ions above the state of $^4I_{13/2}$. As a result, cerium ions act as limiter ions that prevent the up-conversion process in a nanoparticle. Thus, in nanoparticles co-doped with Er^{3+}, Yb^{3+}, Ce^{3+} ions, the maximum excitation efficiency is achieved with subsequent radiative disintegration at a wavelength of 1530 nm.

To shield ions in a nanocrystal from external quenching factors and reduce the effect of surface defects, it is required to create an inert shell on the surface of nanoparticles [25]. The creation of an inert crystalline shell on the surface of nanoparticles with a thickness of more than 5 nm allows to avoid the outflow of excitation energy, which, as a consequence, increases their quantum efficiency.

A number of nanocrystals with various fluoride matrices $NaYF_4:Yb^{3+}$, Er^{3+}, $NaLuF_4:Yb^{3+}$, Er^{3+} and $NaLuF_4:Yb^{3+}$, Er^{3+}, Ce^{3+} were synthesized by the method of high-temperature decomposition of trifluoroacetates in an oxygen-free environment. To improve their photoluminescent properties, the resulting nanoparticles were additionally coated with inert crystalline shells corresponding to the crystalline matrix of the core. As a result, narrowly dispersed nanoparticles with a core/shell structure were obtained. The sizes and morphology of the nanocrystals were characterized using a transmission electron microscope (TEM). The phase composition of nanoparticles was studied by X-ray powder diffraction (XRD) in the range of angles $10^\circ \leq 2\theta \leq 100^\circ$ with a scanning step of 1°. Fig. 2 shows TEM photographs, histograms of the size distribution of

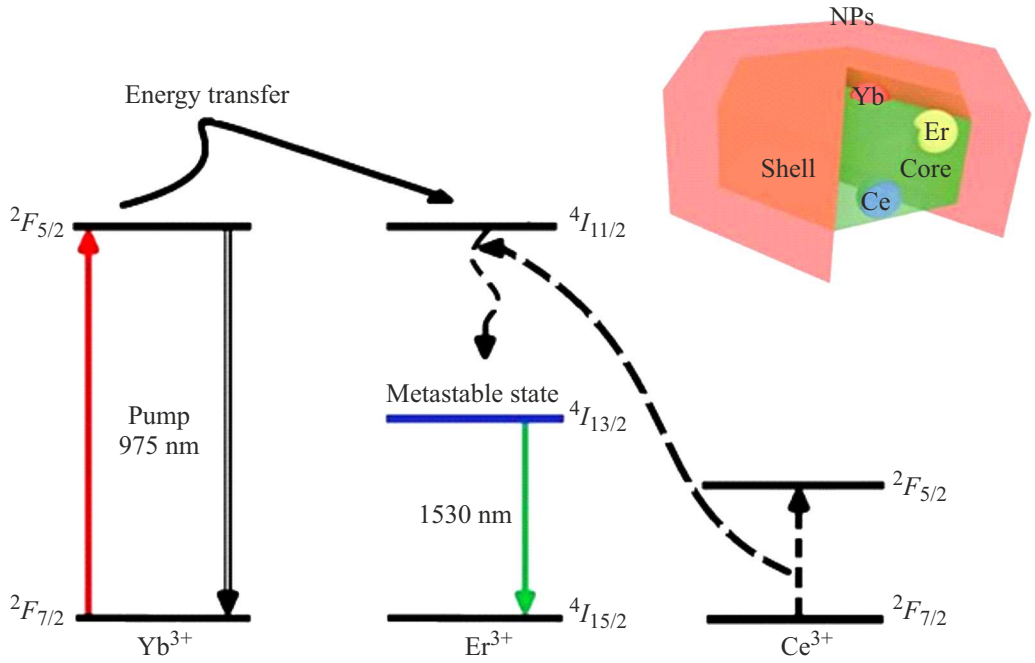

Figure 1. Schematic representation of an individual crystalline nanoparticle with a core/shell structure co-doped with Yb^{3+}, Er^{3+}, Ce^{3+} ions, and an energy level diagram explaining the mechanism of nanoparticle photoluminescence. The Yb^{3+} ion resonantly absorbs radiation at a wavelength of 975 nm and passes into an excited state. The excited Yb^{3+} ion nonradiatively transfers energy to the nearby Er^{3+} ion, transferring it to the excited state $^4I_{11/2}$. The Ce^{3+} ion, due to nonradiative energy transfer, is able to deexcite the Er^{3+} ion to the $^4I_{13/2}$ state, which allows to limit the quantum system for excitation of higher-lying states of the Er^{3+} ion. Thus, in a nanoparticle simultaneously doped with Yb^{3+}, Er^{3+}, Ce^{3+} ions, photoluminescence with a stokes shift in the vicinity of 1530 nm is predominantly realized.

the synthesized nanoparticles, and the corresponding XRD spectra. It can be seen from the obtained photographs that all the synthesized nanoparticles have an average size of 26 to 30 nm and have a high monodispersity in size ± 5 nm. Comparison of the obtained XRD spectra with the known tabular data (ICDD PDF 00-027-0726 and 00-064-0156) allows to conclude that the synthesized nanocrystals have a hexagonal crystalline phase.

Based on the analysis of literature data [3,30,31], the optimal concentration of rare-earth ions in fluoride matrices was chosen: Yb^{3+} — 20%, Er^{3+} — 2% and Ce^{3+} — 2%. The study of the photoluminescence spectra of nanoparticles was carried out on a Fluorolog 3 spectrofluorimeter (HJY, France) with excitation by a semiconductor laser with a wavelength of 975 nm. The luminescence spectrum measured at room temperature is characterized by an intense photoluminescence line with a maximum at a wavelength of 1530 nm From the spectra and photographs of colloidal solutions of nanoparticles shown in Fig. 3, *a*, it can be seen that β-$NaLuF_4$ nanoparticles have the highest photoluminescence intensity in the spectral C-range: Er^{3+}, Yb^{3+}, Ce^{3+}/$NaLuF_4$. The measurement of the absolute quantum efficiency of photoluminescence of the synthesized nanoparticles in the wavelength range 1400–1700 nm was carried out using an integrating sphere.

The dependences of the measured values of the quantum efficiency of colloidal solutions of nanoparticles in decalin on the power density of the exciting radiation at a wavelength of 975 nm are shown in Fig. 3, *b*. The values of the quantum efficiency of the luminescence of the samples at a power density of exciting radiation of 0.6 W/cm^2 varied from 17 to 27.5%. The use of the β - β-$NaLuF_4$ matrix compared to β-$NaYF_4$, recognized as the „standard“ for up-converting nanoparticles, allowed to increase the PL quantum efficiency from 22 to 27.5%. The introduction of cerium ions into the nanocrystal matrix allowed to increase the efficiency of the $^4I_{13/2} \rightarrow {}^4I_{15/2}$ transition by 10% due to the suppression of the up-conversion effect in nanoparticles.

3.2. Waveguide amplifier for telecom C-band wavelengths

Erbium fiber amplifiers, invented in the 1990s, are widely used in modern fiber optic communication lines. The disadvantage of such amplifiers is their length (8–12 m), due to the relatively low concentration of erbium ions in the quartz matrix [32]. At the present time, in connection with the development of integrated optics, the task of creating compact waveguide amplifiers for the telecommunication C-band (1525–1565 nm) that can be integrated into various photonic devices [33] is topical. One of the most promising approaches to the creation of compact 1.5 μm waveguide amplifiers is the incorporation of fluoride nanocrystals co-doped with Yb^{3+}, Er^{3+} ions into a polymer waveguide [34,35].

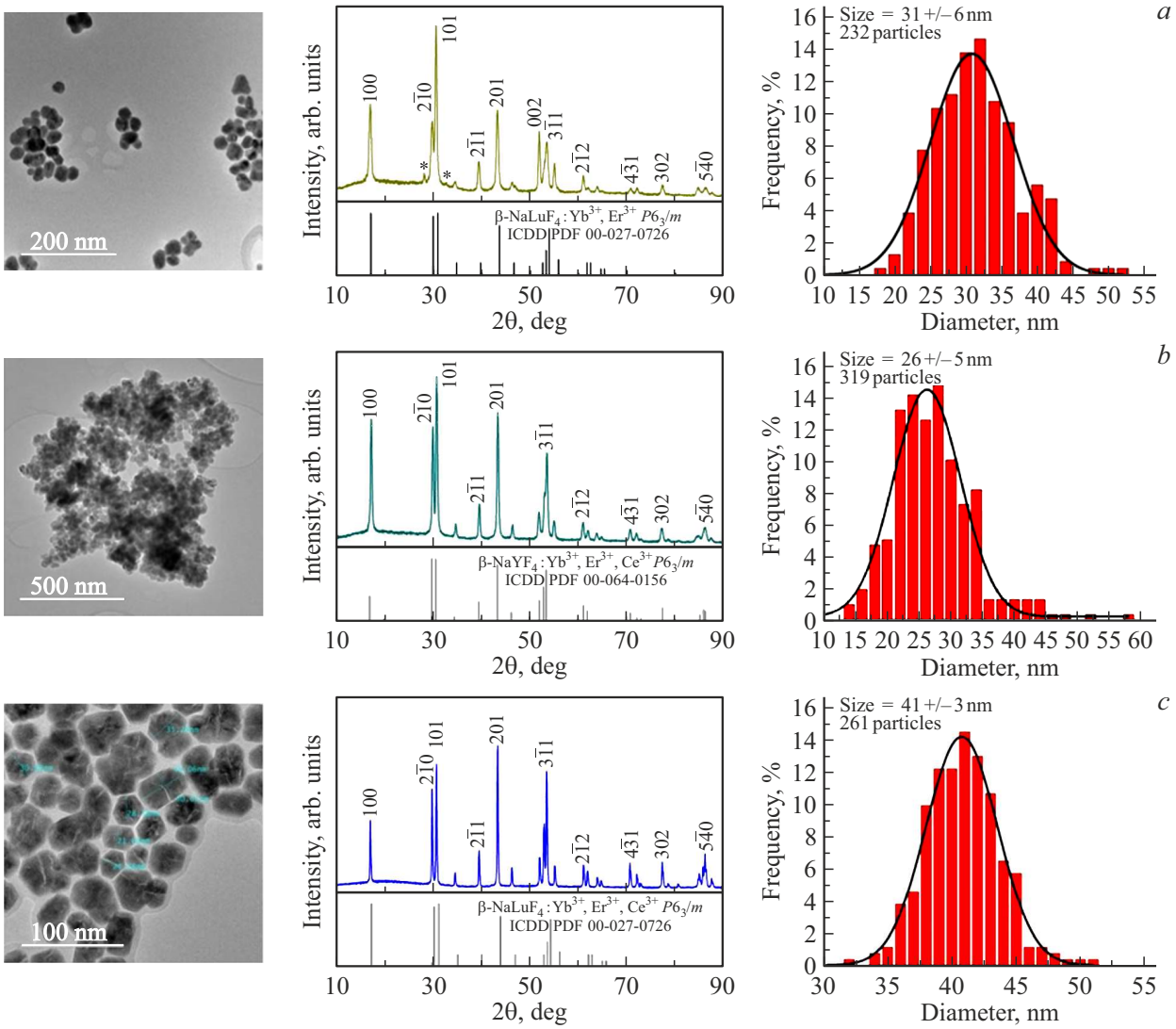

Figure 2. TEM photographs of the synthesized nanoparticles with a core/shell structure, XRD spectra and corresponding histograms of the size distribution of nanoparticles: (*a*) *β*-$NaLuF_4$: Yb^{3+}, Er^{3+}/$NaLuF_4$, (*b*) *β*-$NaYF_4$: Yb^{3+}, Er^{3+}, Ce^{3+}/$NaYF_4$ and (*c*) *β*-$NaLuF_4$:Yb^{3+}, Er^{3+}, Ce^{3+}/$NaLuF_4$.

Nanoparticles $NaLuF_4$:Yb^{3+}, Er^{3+}, Ce^{3+}/$NaLuF_4$ were used to create a polymeric waveguide amplifier for telecommunications C-band. For this, $NaLuF_4$:Yb^{3+}, Er^{3+}, Ce^{3+}/$NaLuF_4$ nanoparticles were dispersed in commercial SU-8 photoresist at a concentration of 0.12 wt.%. Photoresist SU-8 has a high degree of optical transparency in the wavelength range $1.3-1.5\,\mu$m [35]. Polymeric waveguides were manufactured from the obtained nanocomposite material by contact photolithography on a silicon wafer with an oxide layer. The waveguide shell was formed from thermoplastic polystyrene. The width of the light-guiding strands of the polymer waveguides was $8\,\mu$m, the height was $4\,\mu$m, and the length of the waveguides in the array was 15 mm (Fig. 4, *a*). To estimate the optical losses in a waveguide containing inclusions of nanoparticles, the method of successive cutoff [36] was used.

A semiconductor laser with a wavelength of 850 nm was used as a signal source for measuring losses. Laser radiation was started through the polished end of the waveguide using an optical fiber with a core size of $5.4\,\mu$m, and an optical fiber was also attached to the output end of the waveguide. The output signal that passed through the entire length of the nanocomposite waveguide was recorded by a high-speed oscilloscope signal power meter (DTG 5334 Tektronix, USA). By successively cleaving the polymer waveguide to a length of ~ 2 mm and then measuring the intensity of the transmitted signal at a wavelength of 850 nm, it was found that the attenuation coefficient is ~ 0.36 dB/cm, and the loss coefficient for input-output radiation is $K = 0.61$. Fig. 4, *b* shows a photograph of the end face of an array of polymeric waveguides, where light with a wavelength of 1530 nm propagates along one of the waveguides with mode localization inside the light-guiding core.

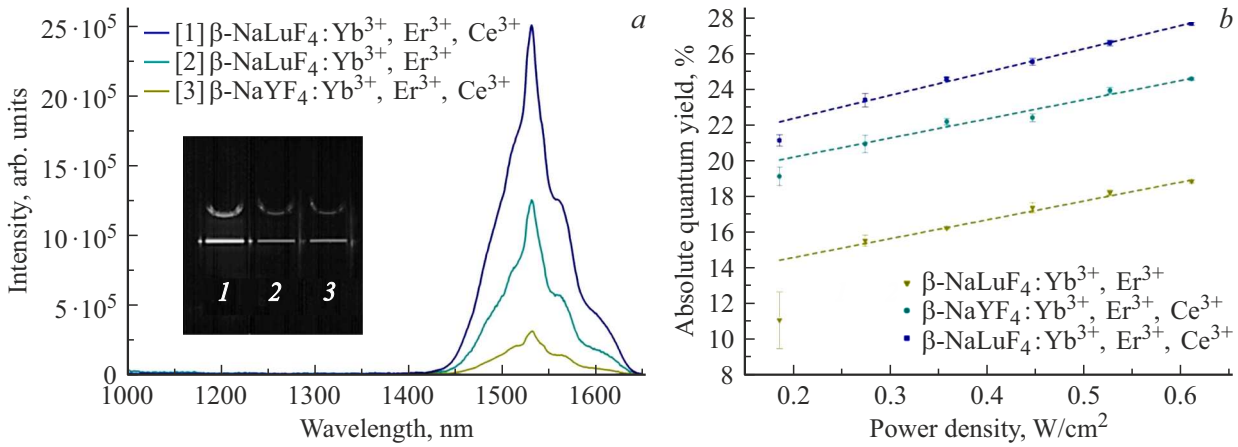

Figure 3. (*a*) Photoluminescence spectrum of the synthesized nanoparticles upon excitation by laser radiation at a wavelength of 975 nm. In the photoluminescence spectrum of nanoparticles, an intense line of the Er^{3+} $^4I_{13/2} \rightarrow {}^4I_{15/2}$ transition is recorded with a maximum at a wavelength of 1530 nm. The insert shows a photograph of colloids of nanoparticles (*1* — β-$NaLuF_4$: Er^{3+}, Yb^{3+}, Ce^{3+}/$NaLuF_4$, *2* — β-$NaLuF_4$: Er^{3+}, Yb^{3+}/$NaLuF_4$, *3* — β-$NaYF_4$: Er^{3+}, Yb^{3+}, Ce^{3+}/$NaYF_4$), obtained using an InGaAs camera that detects a signal in the range from 1000–1700 nm. (*b*) Dependences of the quantum efficiency of nanoparticles at a wavelength of 1400–1700 nm on the power density of the radiation exciting photoluminescence at a wavelength of 975 nm.

The optical gain was measured in the forward direction using the experimental setup shown in Fig. 4, *c*. The gain in the waveguide amplifier was measured using a Santec TSL-550 tunable semiconductor laser as a signal source and a cw laser diode with a wavelength of 975 nm as a pumping source for nanoparticles connected to the light-guiding core of the waveguide. A WDM 980/1550 nm multiplexer was used to combine the input optical signal and pumping radiation. The amplified output signal was collected from the end of the waveguide through a single-mode fiber (Thorlabs 980/1550) with a light-guiding core size of 5.4 μm, which, in turn, was connected to an Anritsu MS9710A optical spectrum analyzer. The amplification of a signal with a wavelength of 1530 nm in the waveguide was calculated by the formula

$$G = 10 \lg \frac{I_{\text{signal+pump}} - I_{\text{pump}}}{I_{\text{signal}}},$$

where $I_{\text{signal+pump}}$ — intensity of the amplified signal at the output from the waveguide with pumping on, I_{pump} — intensity at the output with no amplified signal, I_{signal} — intensity of the signal at the output to the waveguide without pumping.

It can be seen from Fig. 4, *d* that the introduction of $NaLuF_4$: Yb^{3+}, Er^{3+}, Ce^{3+}/$NaLuF_4$ nanoparticles into the polymer waveguide provides amplification of the signal at a wavelength of 1530 nm. At a pumping power of 150 mW in a waveguide polymer amplifier (8 × 4 μm, length 1.5 cm), the gain at a wavelength of 1530 nm was 2.3 dB/cm.

Thus, the use of this class of nanoparticles allows to create compact waveguide amplifiers from polymer photoresists using standard photolithography technology.

3.3. Visualization of nanoparticles in delayed registration mode

Improvement of bioimaging methods requires a transition to a new class of markers with a fluorescence wavelength in the near-IR area of the spectrum. The transition is justified due to the lower light scattering coefficient of biological tissues in the range from 1000 to 1700 nm compared to the spectral range up to 1000 nm. Therefore, new organic fluorochromes are being actively developed and synthesized, the fluorescence edge of which partially captures the near-IR range of the spectrum. An example is the indocyanine green (ICG) dye and its derivatives, which are used in clinical practice [37]. However, poor chemical stability and solubility, as well as an extremely low luminescence quantum efficiency significantly limit the possibilities of bioapplications of organic dyes [38]. The creation of inorganic nanomarkers capable of fluorescing in the near-IR area of the spectrum is extremely important for the development of the fluorescence imaging method [39].

Usually, to register a photoluminescent signal, the method of spectral filtering of the wavelength of excitation and luminescence of nanomarkers is used. In case of nanoparticles with a long lifetime of the excited state, the method of delayed registration is applicable [40]. One of the advantages of this method is the opportunity of recording a photoluminescence signal in a wide range of the spectrum, which depends only on the spectral sensitivity of the camera. It should be noted that time selection is able to provide complete separation of the image of single molecular labels from spurious signals [41].

A specialized visualization system was created that is capable of recording photoluminescence signals from nanomarkers in the near-IR spectral range (Fig. 5, *b*). In the setup, an InGaAs camera was used to record

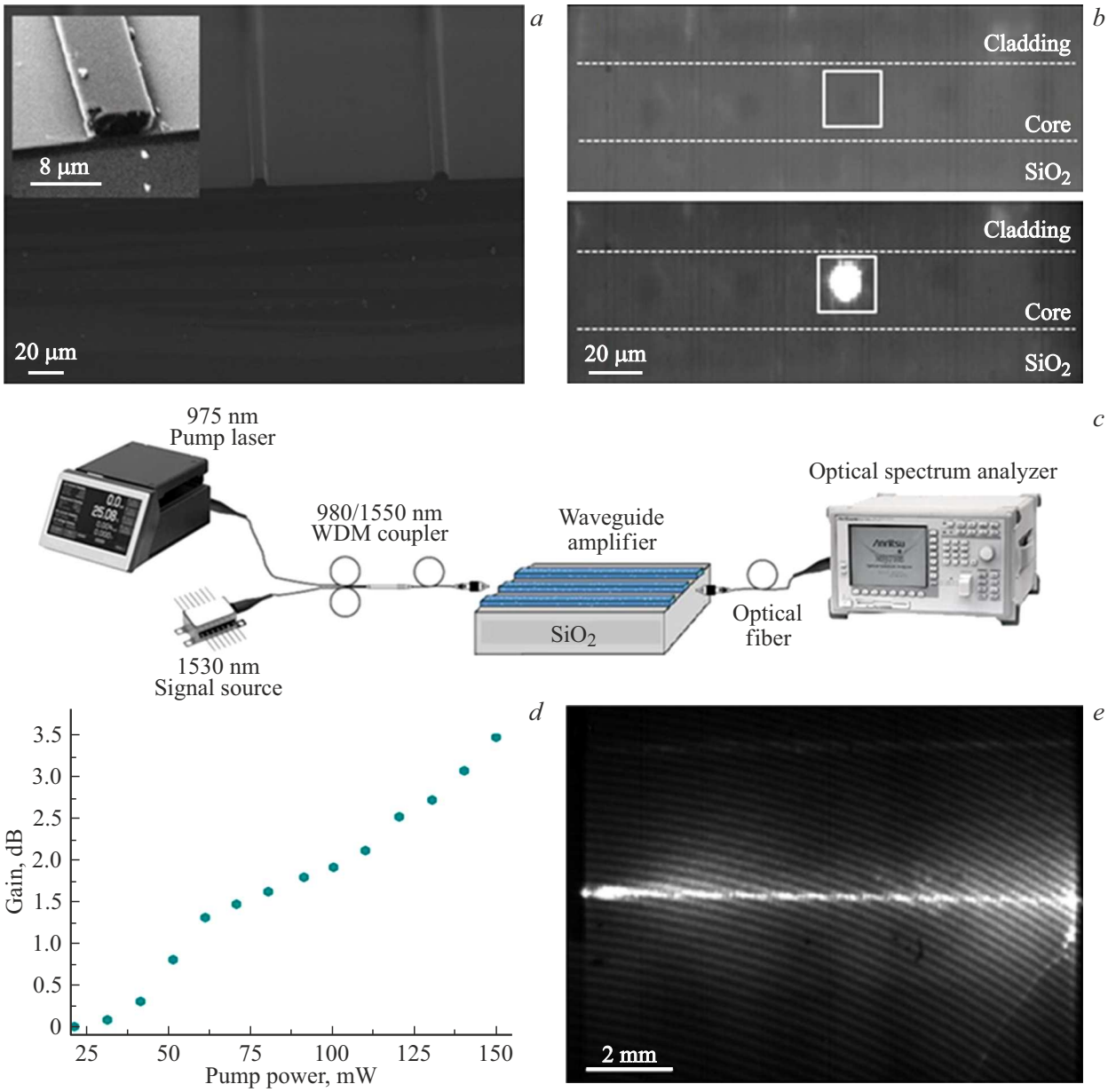

Figure 4. (*a*) SEM microscopy of arrays of single-mode nanocomposite polymeric waveguides with inclusions of $NaLuF_4:Yb^{3+}$, Er^{3+}, $Ce^{3+}/NaLuF_4$ nanocrystals before they are covered with a polystyrene layer. The insert shows an enlarged photograph showing the end face of the waveguide. (*b*) Micrograph of the end face of an array of polymeric waveguides on a silicon substrate after covering them with polystyrene without input of radiation (top) and with input of laser radiation at a wavelength of 1530 nm (bottom). (*c*) Diagram of an experimental setup for measuring the optical gain in a waveguide amplifier. (*d*) Optical amplification of a signal at a wavelength of 1530 nm in a polymer single-mode waveguide with a length of 1.5 cm depending on the pumping power at a wavelength of 975 nm. (*e*) Polymer single-mode waveguide amplifier on a silicon substrate, top view.

the photoluminescence signal from nanoparticles. The system is transluminescent, i.e. the source that excites the photoluminescence of nanoparticles and the receiver that detects the signal are located on opposite sides of the object under study. The diverging laser beam uniformly illuminated the object under study at a wavelength of 975 nm. $NaLuF_4$ nanoparticles were used as markers: Yb^{3+}, Er^{3+}, $Ce^{3+}/NaLuF_4$, having the highest luminescence quantum efficiency. The lifetime of the excited state of ions Er^{3+} ($^4I_{13/2}$) was 8.1 ms (Fig. 5, *a*). The long lifetime of the $^4I_{13/2} \rightarrow {}^4I_{15/2}$ transition allowed to use an optical-mechanical interrupter (chopper) in the delayed registration system. The chopper was installed between the lens and the InGaAs matrix, the maximum modulation frequency was 200 Hz. With the help of a pulse generator, synchronization of time windows of pulsed excitation with a wavelength of

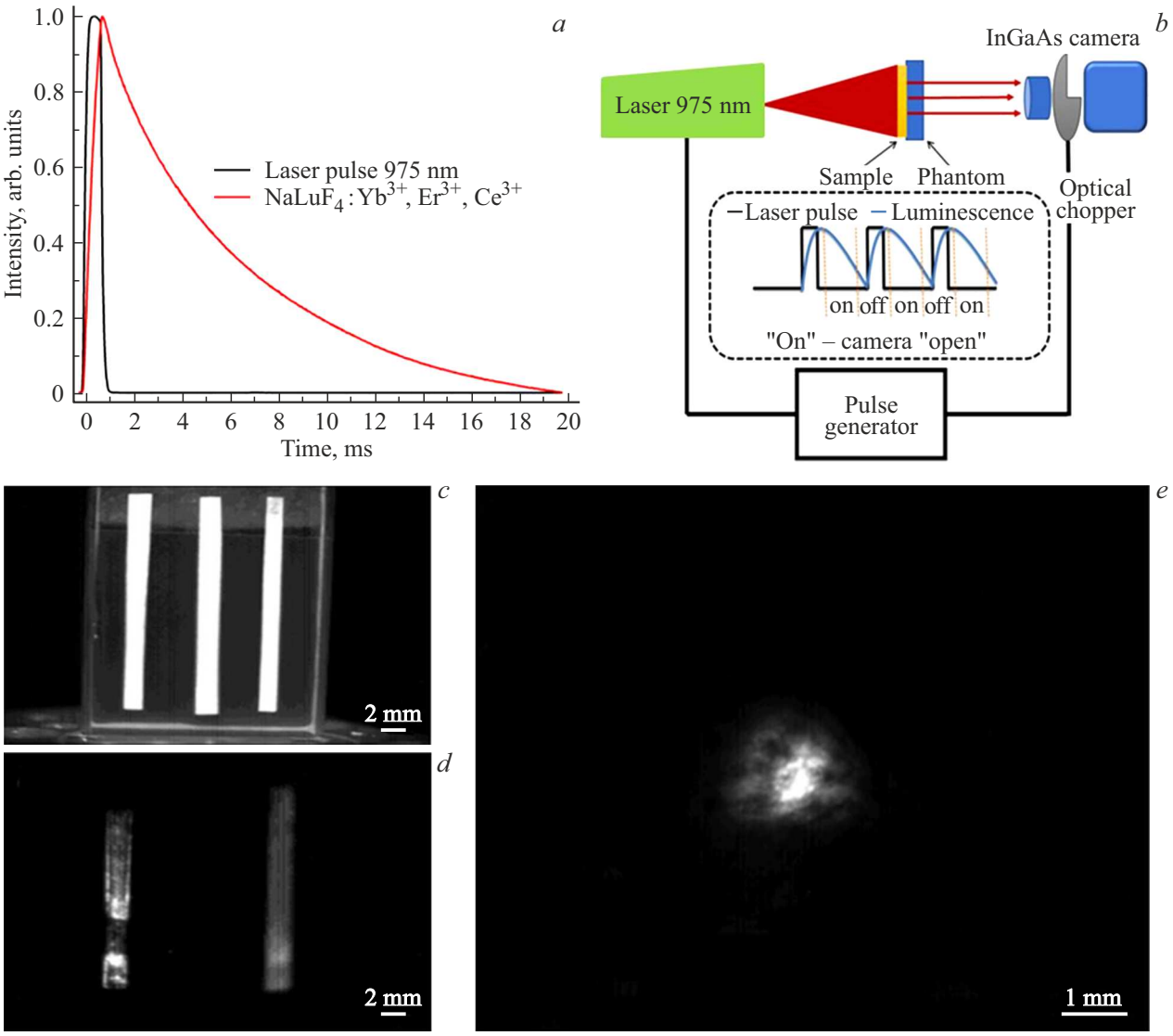

Figure 5. (*a*) Kinetics of photoluminescence of nanoparticles $NaLuF_4:Yb^{3+}$, Er^{3+}, $Ce^{3+}/NaLuF_4$ at a wavelength of 1530 nm upon excitation by a laser pulse with a duration of 1 ms (red curve — kinetics of the disintegration of the $^4I_{13/2} \rightarrow {}^4I_{15/2}$ transition into Er^{3+}, black curve — laser pulse 975 nm). (*b*) Scheme of an imaging system with delayed registration of the photoluminescence signal from nanoparticles. The insert shows the synchronization of the time windows of excitation by laser pulses and the opening of the camera matrix. Adjustment of the synchronization of the laser excitation pulse and registration of the InGaAs camera using test strips: (*c*) lack of synchronization, (*d*) achievement of synchronization. (*e*) Visualization of a dot marker from under a layer of biological tissue.

975 nm and registration of a photoluminescence signal at a wavelength with a maximum of 1530 nm was achieved. The clock delay allowed the laser radiation and background signals with short lifetimes to decay before the luminescence signal from the nanoparticles was obtained. The opening time of the InGaAs matrix by the optomechanical modulator was 750 μs with a signal detection time window of 15 μs, which allowed to detect almost completely the useful fluorescence signal from nanomarkers without the use of spectral filtering devices.

To adjust the system synchronization time windows, an experiment was carried out to record the signal from three paper strips, two of which were impregnated with nanoparticles (Fig. 5, *c, d*). In the absence of the required synchronization between the laser excitation pulse and the luminescence signal, three markers were recorded in the image from the InGaAs camera (Fig. 5, *c*). When the desired synchronization was reached, the laser excitation pulse had time to decay completely, and only markers impregnated with nanoparticles were visualized in the image (Fig. 5, *d*).

The opportunity of visualization of nanoparticles from under a layer of biological tissue was demonstrated. To do this, the nanoparticles were introduced into the polymer, from which a dot marker with a diameter of 500 μm m was made. The marker was inserted into the chicken thigh

to a depth of 4 mm. Fig. 5, *e* shows the visualization of a point marker in the near-IR range of the spectrum in the delayed registration mode. Thus, it was shown that the use of this class of nanoparticles allows to implement a delayed registration mode in the near-IR area of the spectrum, expanding the opportunities of methods for visualizing biological objects.

4. Conclusion

Narrowly dispersed $NaRF_4(R = Y, Lu)$ nanoparticles codoped with Yb^{3+}, Er^{3+}, Ce^{3+} ions were synthesized by the method of thermal decomposition of precursors. The photoluminescence spectrum of nanoparticles excited by laser radiation with a wavelength of 975 nm, measured at room temperature, is characterized by an intense line with a maximum at a wavelength of 1530 nm. Direct measurements of the luminescence quantum efficiency showed that nanoparticles with a core/shell structure of the form $NaLuF_4:Yb^{3+}$, Er^{3+}, $Ce^{3+}/NaLuF_4$ have the highest efficiency. The efficiency of the quantum efficiency of the $^4I_{13/2} \rightarrow {}^4I_{15/2}$ Er^{3+} transition was estimated at 28% at an excitation intensity of 0.6 W/cm^2.

Nanoparticles were used to create a polymeric waveguide amplifier of telecommunications C-band. Light-guiding strands of a waveguide amplifier with transverse dimensions $8 \times 4\,\mu$m were formed from the SU-8 photoresist (with introduced nanoparticles) by contact photolithography. The sheath of light-guiding conductors was formed from polystyrene. At a pump power of 150 mW at a wavelength of 975 nm in a waveguide 1.5 cm long, a gain of 2.3 dB/cm was obtained at a wavelength of 1530 nm. The high quantum efficiency of the synthesized nanocrystals and the long lifetime of the ~ 8 ms transition of the $^4I_{13/2} \rightarrow {}^4I_{15/2}$ transition allowed to implement a background-free optical imaging system with a time delay, in which an optical-mechanical interrupter was used to separate the laser excitation and the photoluminescence signal.

Using an InGaAs camera, the opportunity of visualizing nanoparticles at a wavelength of 1530 nm from under a 4 mm layer of biological tissue was demonstrated.

Acknowledgments

The authors of the work express their gratitude to the staff of the FSRC „KiF“ RAS: A.V. Koshelev for help in recording and interpreting the XRD spectra of nanoparticles, and I.O. Goryachuk for help in measuring the quantum efficiency of nanoparticle luminescence.

Funding

This study was supported financially by the Ministry of Science and Higher Education of the Russian Federation: Agreement № 075-15-2021-1357 regarding „the creation of a waveguide amplifier for telecommunication C-band wavelengths“ and the Russian Science Foundation (Project No. 21-79-10384) regarding „Visualization of nanoparticles in near-IR spectrum“. In the „part of the synthesis of nanoparticles and the study of their photoluminescent properties“ the article was prepared as part of the paper on the topic „Laser technologies for biomedical applications“ (№ 12212260055-2) under the state assignment of the Ministry of Education of the Russian Federation.

Conflict of interest

The authors declare that they have no conflict of interest.

References

[1] D. Hao, D. Shuo-Ren, Z. Xiao-Yu, L. Guang-Ming, S. Ling-Dong, L. Lin-Dong, Z. Pei-Zhi, Z. Chao, Y. Chun-Hua. Chem. Rev., **115**, 10725–10815 (2015). DOI: 10.1021/acs.chemrev.5b00091

[2] D.N. Karimov, P.A. Demina, A.V. Koshelev, V.V. Rocheva, A.V. Sokovikov, A.N. Generalova, V.P. Zubov, E.V. Khaydukov, M.V. Kovalchuk, V.Y. Panchenko. Nanotechnol. Russia, **15**, 655–678 (2020). DOI: 10.1134/S1995078020060117

[3] Y. Zhong, H. Dai. Nano Res., **13**, 1281–1294 (2020). DOI: 10.1007/s12274-020-2721-0

[4] A.N. Generalova, B.N. Chichkov, E.V. Khaydukov. Adv. Colloid Interface Sci., **245**, 1–19 (2017). DOI: 10.1016/j.cis.2017.05.006

[5] G. Liu. Springer Series in Materials Science, **83**, 1–94 (2005). DOI: 10.1007/3-540-28209-2_1

[6] A. Nadort, J. Zhao, E.M. Goldys. Nanoscale, **8** (27), 13099–13130 (2016). DOI: 10.1039/C5NR08477F

[7] F. Wang. Chem. Soc. Rev., **38** (4), 976 (2009). DOI: 10.1039/B809132N

[8] L.C. Ong. Lumin., **25** (4), 290–293 (2010). DOI: 10.1007/s13404-017-0221-0

[9] E.A. Grebenik, A.B. Kostyuk, S.M. Deyev. Russian Chem. Rev., **85** (12), 1277 (2016). DOI: 10.1070/RCR4663

[10] M. Kaiser, C. Würth, M. Kraft, I. Hyppänen, T. Soukka, U. Resch-Genger. Nanoscale, **9** (28), 10051–10058 (2017). DOI: 10.1039/C7NR02449E

[11] E.V. Khaydukov, K.E. Mironova, V.A. Semchishen, A.N. Generalova, A.V. Nechaev, D.A. Khochenkov, E.V. Stepanova, O.I. Lebedev, A.V. Zvyagin, S.M. Deyev, V.Ya. Panchenko. Sci. Rep., **6**, 35103 (2016). DOI: 10.1038/srep35103

[12] S. Kuznetsov, Yu. Ermakova, V. Voronov, P. Fedorov, D. Busko, I.A. Howard, B.S. Richards, A. Turshatov. J. Mat. Chem. C, **6** (3), 598–604 (2018). DOI: 10.1039/c7tc04913g

[13] E. Madirov, S.V. Kuznetsov, V.A. Konyushkin, A.N. Nakladov, P.P. Fedorov, Th. Bergfeldt, D. Hudry, D. Busko, I.A. Howard, B.S. Richards, A. Turshtov. J. Mater. Chem. C, **9**, 3493–3503 (2021). DOI: 10.1039/D1TC00104C

[14] E. Downing. Science, **273** (5279), 1185–1189 (1996). DOI: 10.1126/science.273.5279.118

[15] R. Deng. Nature Nanotechnology, **10**, 237–242 (2015). DOI: 10.1038/nnano.2014.317

[16] M. Kumar. Biosens. Bioelectron., **25**, 2431–2435 (2010). DOI: 10.1016/j.bios.2010.03.038

[17] K.K. Green, W. Janina, F. Shuang. Scientific Reports, **7**, 762 (2017). DOI: 10.1038/s41598-017-00869-3

[18] E.V. Khaydukov, V.V. Rocheva, K.E. Mironova. Nanotechnol. Russia, **10**, 904–909 (2015). DOI: 10.1134/S1995078015060051
[19] J.M. Meruga, W.M. Cross, P.S. May, Q. Luu, G.A. Crawford, J.J. Kellar. Nanotechnology, **23** (39), 395201 (2012). DOI: 10.1088/0957-4484/23/39/395201
[20] S.Y. Hao, D. Shang, H. Li, C. øAgren, C. Yang, G. Chen. Nanoscale, **9** (6), 6711–6715 (2017). DOI: 10.1039/C7NR01008G
[21] V.V. Rocheva, A.V. Koroleva, A.G. Savelyev, K.V. Khaydukov, A.N. Generalova, A.V. Nechaev, A.E. Guller, V.A. Semchishen, B.N. Chichkov, E.V. Khaydukov. Scientific Reports, **8**, 3663 (2018). DOI: 10.1038/s41598-018-21793-0
[22] Q. Zhan, H. Liu, B. Wang, Q. Wu. Nature Commun., **8**, 1058 (2017). DOI: 10.1038/s41467-017-01141-y
[23] E.V. Khaydukov, V.A. Semchishen, A.V. Zvyagin. Opt. Lett., **40** (7), 1169–1172 (2015). DOI: 10.1364/OL.40.001169
[24] M. Wang, Y. Zhu, C. Mao. Langmuir, **31**, 7084–7090 (2015). DOI: 10.1021/la204015m
[25] G. Chen, H. Qiu, P.N. Prasad, X. Chen. Chem. Rev., **114** (10), 5161–5214 (2014). DOI: 10.1021/cr400425h
[26] X. Chen, Y. Zhu, D. Zhou, W. Xu, J. Zhu, G. Pan, Z. Yin, H. Wang. J. Mater. Chem., **5**, 2451 (2017). DOI: 10.1039/C2JM34273A
[27] I.V. Krylov, R.A. Akasov, V.V. Rocheva, N.V. Sholina, D.A. Khochenkov, A.V. Nechaev, N.V. Melnikova, A.A. Dmitriev, A.V. Ivanov, A.N. Generalova, E.V. Khaydukov. Front. Chem., **8**, 295 (2020). DOI: 10.3389/fchem.2020.00295
[28] D. Wang, P. Ma, J. Zhang, Y. Wang. ACS Applied Energy Materials, **1** (2), 447–454 (2018). DOI: 10.1021/acsaem.7b00093
[29] Y. Zhong, Z. Ma, S. Zhu. Nat. Commun., **8**, 737 (2017). DOI: 10.1038/s41467-017-00917-6
[30] X. Zhai, J. Li, S. Liu, X. Liu, D. Zhao, F. Wang, D. Zhang, G. Qin, W. Qin. Opt. Mater. Express, **3**, 270–277 (2013). DOI: 10.1364/OME.3.000270
[31] C. Cao, Y. Xie, S.-W. Li, C. Hong. Nanomaterials, **11**, 2676 (2021). DOI: 10.3390/nano11102676
[32] R.G. Smart, J.L. Zyskind, D.J. DiGiovanni. IEEE Photon. Technol. Lett., **5** (7), 770–773 (2002). DOI: 10.1364/JOSAB.21.000739
[33] H. Gao, H. Li, G.F.R. Chen. Sci. Rep., **11**, 21292 (2021). DOI: 10.1038/s41598-021-00805-6
[34] X. Zhai. Opt. Mater. Express, **3**, 270–277 (2013). DOI: 10.1364/AO.53.006148
[35] P.C. Zhao, M.L. Zhang, T.J. Wang, X.Y. Liu, X.S. Zhai, G.S. Qin, W.P. Qin, F. Wang, D.M. Zhang, J. Nanomater., **2014**, 153028 (2014). DOI: 10.1155/2014/153028
[36] A.Q. Quang, R. Hierle, J. Zyss, I. Ledoux, G. Cusmai, R. Costa, A. Barberis, S.M. Pietralunga. Appl. Phys. Lett., **89**, 141124 (2006). DOI: 10.1063/1.2360179
[37] C. Alius, S. Oprescu, C. Balalau, A. Elena Nica. J. Clin. Invest. Surg., **3**, 1–8 (2018). DOI: 10.25083/2559.5555/31.18
[38] H.M. Gil, T.W. Price, K. Chelani, J.-S.G. Bouillard, S.D.J. Calaminus, G.J. Stasiuk. iScience, 24, 102189 (2021). DOI: 10.1016/j.isci.2021.102189
[39] W. Li, G. Zhang, L. Liu. Front Bioeng. Biotechnol., **26** (9), 768927 (2021). DOI: 10.3389/fbioe.2021.768927.
[40] E.V. Khaydukov, K.N. Boldyrev, K.V. Khaydukov, I.V. Krylov, I.M. Asharchuk, A.G. Savelyev, V.V. Rocheva, D.N. Karimov, A.V. Nechaev, A.V. Zvyagin. Opt. Spectrosc., **126**, 95–101 (2019). DOI: 10.1134/S0030400X19010077
[41] J. Yuan, G. Wang. TrAC Trends in Analytical Chemistry, **25** (5), 490–500 (2006). DOI: 10.1016/j.trac.2005.11.013

Translated by E.Potapova